Project funded by the Horizon 2020

Grant Agreement no. 829010

PRIME

Call: H2020-FETOPEN-2018-2020
Topic: FETOPEN-01-2018-2019-2020
Type of Action: RIA (Research and Innovation action)
Name of Lead Beneficiary: CSIC, Spain
Project Start Date: 1st May 2019
Project Duration: 48-Months

DELIVERABLE 1.2:
First round of sensing printable materials

Due date of Deliverable:	30/04/2020
Actual Submission Date:	**29/04/2020**
Responsible partner:	TU/e
Report Author(s):	Alberto F. Belmonte Parra, Dirk Jan Mulder, Isabel Mendiara, Carlos Sánchez-Somolinos, Jesús Martínez de la Fuente
Type1[1]:	R
Dissemination Level[2]:	CO

[1] **Type**: Use one of the following codes (in consistence with the Description of the Action):
- R: Document, report (excluding the periodic and final reports)
- DEM: Demonstrator, pilot, prototype, plan designs
- DEC: Websites, patents filing, press & media actions, videos, etc.
- OTHER: Software, technical diagram, etc.

[2] **Dissemination level**: Use one of the following codes (in consistence with the Description of the Action)
- PU: Public, fully open, e.g. web
- CO: Confidential, restricted under conditions set out in the Model Grant Agreement
- CI: Classified, information as referred to in Commission Decision 2001/844/EC

CSIC TU/e Universidad Zaragoza BIO NANONET BEOnChip

DELIVERABLE D1.2: First round of sensing printable materials

Table of Contents

1 Document History....3
2 List of Abbreviations....4
3 Deliverable Description and Summary....5
4 Introduction....7
4.1 Objectives and approach....9
4.1.1 Development of an irreversible thermal transducer....9
5 Results....11
5.1 Jettable CLC thermal transducer....11
5.1.1 Design....11
5.1.2 Multi-temperature sensing....15
5.1.3 Time-temperature Dependence....17
5.2 CLC thermal transducer particles....18
5.3 Biofunctionalization and Sensing using CLCs....19
5.3.1 Gold Nanoprisms Synthesis....19
5.3.2 ThermoELISA Sandwich Immunoassay....19
5.3.3 CLC polymer compatibility with the sample treatment....21
5.3.4 CLC polymer ThermoELISA results....22
5.3.5 Optimizing blocking agent for AuNPRs....24
5.3.6 BSA....24
5.3.7 PEG....24
6 Conclusions....27
7 Open Points and Outlook....27
8 References....28

PRIME has received Funding from the European Union's Horizon 2020 research and innovation programme under Grant Agreement No. 829010

1 DOCUMENT HISTORY

Version	Date	Authors/ who took action	Comment	Modifications made by
0.1	08/04/2020	ABP and DJM	First draft sent to CSS and JMdlF (CSIC)	
0.2	12/04/2020	JMdlF, CSS and IMN	Second draft sent to DJM	
0.3	17/04/2020	DJM	Third draft sent to PIs	CSS, JMdlF, and IMN
1.0	29/04/2020	CSS	Submitted to Commission	

Initials used:

ABP Alberto Belmonte Parra (TU/e)

DJM Dirk Jan Mulder (TU/e)

CSS Carlos Sánchez Somolinos (CSIC)

JMdlF Jesús Martinez de la Fuente (CSIC)

IMN Isabel Mendiara Negredo (CSIC)

PRIME has received Funding from the European Union's Horizon 2020 research and innovation programme under Grant Agreement No. 829010

2 LIST OF ABBREVIATIONS

NP	Nanoparticle
CA 19-9	Carbohydrate antigen
VEGF	Vascular endothelial growth factor
CEA	Carcinoembryonic antigen
ELISA	Enzyme-linked immunosorbent assay
SPR	Surface plasmon resonance
RI	Refractive index
IR	Infrared
NIR	Near IR
LSRP	Localized surface plasmon resonance
LC	Liquid crystal
CLC	Cholesteric liquid crystal
T_g	Glass transition temperature
T_{iso}	Isotropization temperature
IPN	Interpenetrating polymer network
BA	Benzyl acrylate
ʎ	Wavelength
UV	Ultraviolet
NCPPS	Non-crosslinked photonic polymer structure
PVA	Poly (vinyl alcohol)
UV-Vis	Ultraviolet-visible spectroscopy
DSC	Differential scanning calorimetry
POM	Polarized optical microscopy
DIW	Direct ink writing

PRIME has received Funding from the European Union's Horizon 2020 research and innovation programme under Grant Agreement No. 829010

3 DELIVERABLE DESCRIPTION AND SUMMARY

PRIME aims to develop a thermal transduction system that can be integrated by printing techniques in a microfluidic device for the quantification of ultralow concentrations of analytes. This technology will make use of detection antibodies coupled to plasmonic nanoparticles (NPs) and analyte-capturing antibodies that will be coupled to a thermoresponsive cholesteric liquid crystal polymer (LCP) layer acting as an optical detection element. The sample with the analyte will diffuse and the signal will be obtained using functionalized NPs that also attach to the analytes. In the presence of analyte an analyte-nanoparticle "sandwich" will be formed on the surface of layer. Irradiation with near-infrared (NIR) light will induce heating of the plasmonic NPs inducing a color change of the cholesteric LCP support, thus operating as a thermal signal transducer (Figure 1).

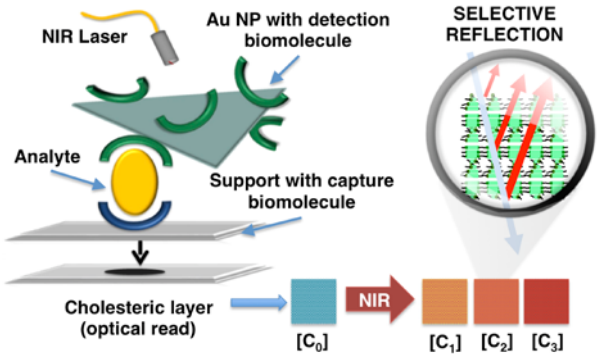

Figure 1, Nanoparticle based sensor with cholesteric thermo-optical transducer.

This report comprises the results of TU/e and CSIC on the design, synthesis, printing, characterization of an initial set of cholesteric formulations leading to thermal transducers and first steps toward their bio-functionalization.

As a first step, the aim is to develop an irreversible thermal transducer that can be fabricated using inkjet printing. Various fabrication approaches were considered including cold programming, hot-embossing, and using non-crosslinked CLC polymers. The latter gave best results in terms of processing and irreversible response. We developed a jettable ink formulation to print coatings with tunable color and detection temperature between ~65 °C and ~85 °C. The response of the coating was driven by the isotropization temperature (T_{iso}). Once the coating is heated above the T_{iso}, the coating loses its order and turns colorless. Once cooled back to room temperature, it forms a scattering focal conic state. Since the scattering state is easy to distinguish from the colorful reflecting state, the user is able the read-out the sensor by simple colorimetric assays. We developed a multi temperature sensor using the developed inks and showed that the materials are stable under aqueous conditions.

Besides the irreversible response, also a gradual red-shift was observed when the coating was exposed to elevated temperatures below T_{iso}. This response could pave way towards a time-temperature integrating (TTI) sensor where the color shift represents the time at which the sensor was held at a certain temperature. During the next reporting period, efforts will be made modelling the TTI response and the development of a TTI sensor. Furthermore, attempts will be made reducing the detection temperature and response time.

PRIME has received Funding from the European Union's Horizon 2020 research and innovation programme under Grant Agreement No. 829010

Also, non-crosslinked CLC polymer particles were synthesized. CLC polymer particles do not exhibit angle-dependent color reflection and do not need alignment layers. These benefits will aid both in the fabrication and read-out of the sensor. The particles can potentially be dispersed in a refractive index (RI) matching binder that can be processed using additive manufacturing (AM) techniques such as Direct Ink Writing (DIW). Preliminary results showed that the particles respond to temperature like the inkjet-printed sensors. However, the initial optical state was already quite scattering caused by RI mismatch between the particles and the binder, and surface roughness. During the next reporting period efforts will be made optimizing both the particles and the binder to be compatible with DIW and reducing scattering in the initial state. Furthermore, anchoring groups will be introduced to the binder to facilitate the bio-functionalization.

Briefly, the biosensor is intended to be an ELISA sandwich built up over the CLC polymer or in close contact with it. This sandwich comprises the immobilization of the capture antibody on the CLC polymer surface, then the addition of the sample containing the antigen and finally, the addition of the bioconjugate, which is the resulting molecule after functionalizing the gold nanoprisms (AuNPs) with the detection antibody. The detection step comprised the irradiation of the biosensor with an NIR laser.

Several experiments were carried out to find the optimal working conditions. It was important to take into account the pKa of the carboxyl groups present in CLC polymer, to meet the suitable pH for the immobilization of other molecules (capture antibodies in this case) and check if the color and structure of the polymer remained stable along with the sample treatment.

This color change was monitored at the beginning and at the end of the ELISA protocol by observing the RGBs of the CLC polymer, using a mobile phone camera. Two different CLC polymers were analyzed. It can be said that they all lose brightness and as a consequence they became greener and bluer. Despite these observations, it was possible to see a temperature increase in the samples, after irradiating the samples containing the complete ELISA sandwich with the laser, meaning that the biosensor was working.

The optimization of several steps of the bioconjugation protocol was carried out. It is important blocking properly the nanoparticle after adding the detection antibody to avoid unspecific interactions with the real sample. Two blocking agents were chosen, namely bovine serum albumin (BSA) and polyethylene glycol (PEG). BSA agent exhibited a reproducible behavior between the three replicates but less temperature increases only 4,5 ºC on average compared to the initial temperature. By contrast, PEG agent exhibited an important temperature increase in all the samples, more than 40 ºC. These results indicated that PEG acts better as a blocking agent than BSA. BSA is a large molecule that can avoid the binding with the antigen in the sample. Finally, it is important to highlight the fact that similar temperature increase was detected irradiating both the functionalized side and the non-functionalized side. This finding opens new possibilities for building up different biosensor configurations.

The next challenges of the project will be focused on building the biosensor on a polymer located between the ELISA sandwich and the CLC polymer. This polymer could be Polydimethylsiloxane (PDMS). It can act as a support that will provide stability to the sensor owing to the separation of the CLC polymer from the ELISA sandwich. The main advantage would be that the optimization of the parameters will only carry out once and the appearance and the structure of the CLC polymer could be preserved intact.

PRIME has received Funding from the European Union's Horizon 2020 research and innovation programme under Grant Agreement No. 829010

4 INTRODUCTION

Sensor technologies have attempted the use of nanoparticles (NPs) containing fluorescent or colorimetric markers. However, the major limitation of nano biosensors based on color/fluorimetric transducers are their low sensitivity, and the presence of false positives induced by another colorant presented in the sample matrix. Usually, complex sample treatments are required to eliminate interferences. This increases the complexity and duration of the assay. These limitations are not present in thermal transducer biosensors, simplifying (or even eliminating) any sample treatment.

As an example, in which sensor technology is highly relevant, gastrointestinal cancers include the cancer of all organs of the digestive system, being some of them the most mortality and nowadays accounts for 20 percent of all diagnosed cancer cases. This is due to the poor prognosis, with low 5-year survival and less than one year in the case of advanced stages.[1] The identification of unique patterns and specific biomarkers is essential to develop accurate diagnostic tools and effective treatments. Until now, the number of effective biomarkers applied in the clinic for the diagnosis of gastric cancer is very low.[2] Some of the most commonly used cancer markers (secreted by cancer cells in the blood or other body fluids) for the diagnosis of colorectal or pancreatic cancer are carbohydrate antigen 19-9 (CA 19-9), vascular endothelial growth factor (VEGF), and carcinoembryonic antigen (CEA).[3,4] These blood tumor markers are currently determined with traditional analytical methods such as enzyme-linked immunosorbent assay (ELISA)[5]. Even so, these markers are not specific, they are not directly related to the type of cancer, since they are at high levels in different cancer pathologies and are not always sensitive markers because sometimes metastatic cases involve non-secretory tumors. [6] That is why the main challenge in the diagnosis of this type of cancer focuses on the one hand on specific detection, through the search of new tumor markers in blood for gastrointestinal cancer and on the other hand, in the early detection, through the development of new methods that allow the detection at low concentrations of these specific markers to which classical methods cannot reach. As a solution to these problems, advances in fields of microelectronics, materials and nanotechnology are being implemented to improve these systems.[7,8]

Currently, many methods use different gold nanoparticle labeling for signal amplification in different sandwich immunosensors and immunoassays[9,10], allowing the recognition of specific biomolecules in ultra-low concentration ranges. Depending on the intrinsic property of the nanoparticle used, we can translate the biological recognition into an electrochemical, mass-sensitive, optical, chemiluminescence, electrochemiluminescence, fluorescence or surface plasmon resonance (SPR) signal.[11] This last property is one of the most used, SPR methods based on gold nanoparticles have recently brought a wide variety of methodologies (sensing, detecting, and imaging) due to their high versatility and their unique tunable optical properties.[12] In addition, plasmonic gold nanoparticles can experience photothermal conversion and be able to convert light energy into heat, which makes them an attractive candidate for photothermal therapy[13–16] , thermoimaging[17,18] and ultimately thermal detection[19,20]. It is also important to know that the anisotropy in this type of nanoparticles changes their optical properties and as a result we can obtain a strong absorption in the near infra-red (IR) range (NIR), after the excitation by the incident light, generating strong local heating by photothermal conversion of light energy absorbed into local heating, what makes these anisotropic gold nanoprisms (AuNPs) extremely efficient for NIR-induced heating. [21–23] AuNPs are ones of these anisotropic nanoparticles, that exhibit tunable localized surface plasmon resonance (LSRP) in the near infrared region (NIR), with sizes> 100 nm, being able transform optical energy (light) into heat in a very effective way.[24]

PRIME has received Funding from the European Union's Horizon 2020 research and innovation programme under Grant Agreement No. 829010

The application of these nanoparticles for detection has already been tested for qualitative/semi-quantitative methods in immunoassays, obtaining high sensitivity, selectivity and specificity.[20]

PRIME will develop an innovative and sensitive thermal transduction system that can be easily integrated by inkjet printing in a microfluidic device for the detection and quantification of ultralow concentrations of a plethora of analytes, including proteins. This sensing technology will use detection antibodies coupled to plasmonic nanoparticles and analyte-capturing antibodies immobilized on a support consisting of a thermosensitive cholesteric liquid crystal (CLC) polymer layer that functions as a photographic detection element. CLC polymers are great candidates to realize novel optical sensors. CLCs are photonic materials exhibiting a photonic bandgap because of the presence of a helical molecular organization[25] (Figure 2). The reflected wavelength (or color) depends on the pitch of the helix that can be easily tuned by the chemical composition and further stabilized by chemical and/or physical crosslinking into a polymer network[26–28]. Such photonic structures have been extensively investigated as optical sensors as they can respond to external stimuli, such as temperature, humidity and light, by changing their optical properties[29–33].

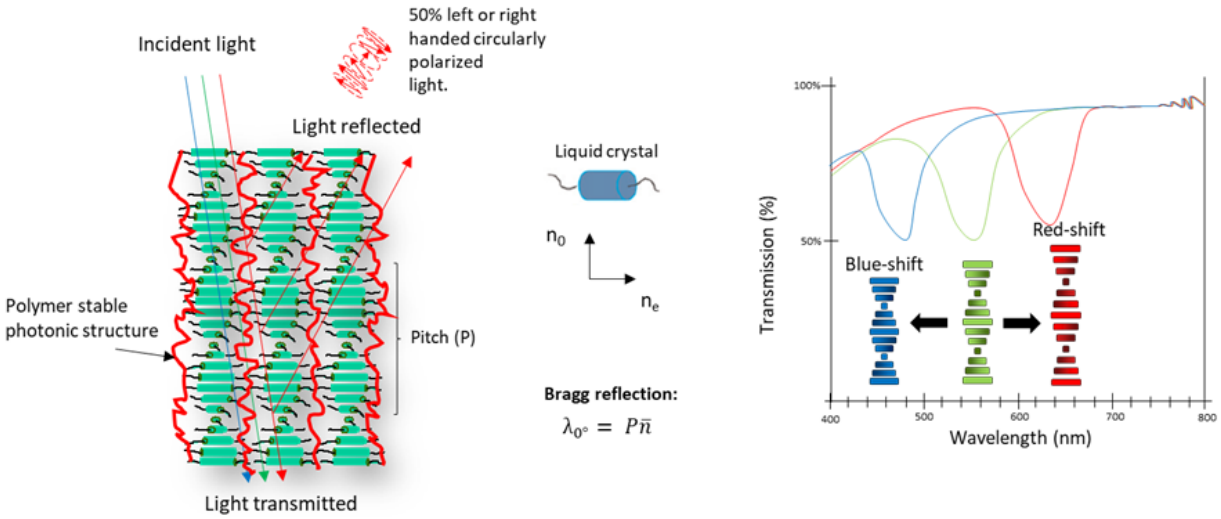

Figure 2. Scheme of the light interaction with a cholesteric liquid crystalline polymer network.

Alternatively, to increase sensitivity a dual-active layer with a top matrix bearing the recognition antibodies will be attached directly on the surface of the cholesteric layer. The sample containing the analyte will diffuse and the signal is obtained using functionalized particles that also attach to the analytes. In the presence of the analyte to be detected, an analyte-nanoparticle "sandwich" will be formed on the surface of the sensors. Irradiation of the area by a near-infrared (NIR) laser source will cause any plasmonic NPs present to release vast amounts of heat, labeling the cholesteric LCP support to produce a color-scale change in the LCP layer, thus operating as a thermal signal transducer. Formulations will be designed to prepare thermal transducers using inkjet printing with special emphasis on irreversible cholesterics that convert the heat in a visible and permanent colour change. The color change will be read using a conventional camera, that will allow quantifying the presence of the analyte down to ultralow concentration range.

PRIME has received Funding from the European Union's Horizon 2020 research and innovation programme under Grant Agreement No. 829010

4.1 Objectives and approach

4.1.1 Development of an irreversible thermal transducer

This research aims to develop a CLC ink that can be printed on the microfluidics device to fabricate temperature sensors. The sensors must show irreversible and relevant optical changes, for instance a color-shift, when the temperature reaches the detection temperature. Here, we design and analyze different approaches to fabricate irreversible thermal sensors with CLC materials, ensuring optimal rheological properties for additive manufacturing.

Solvent-induced cold programming of photonic polymer structure

A temperature sensor based on solvent-induced room-temperature programming of porous CLC polymer coatings is proposed. The CLC porous polymer coating is formed with a reactive CLC mixture containing a non-reactive compound. The non-reactive compound is extracted after polymerization generating a CLC porous polymer network. Collapsing (blue-shift) and recovering the polymer structure is then attained by controlled solvent evaporation or upon exposure to certain solvents (Figure 3).

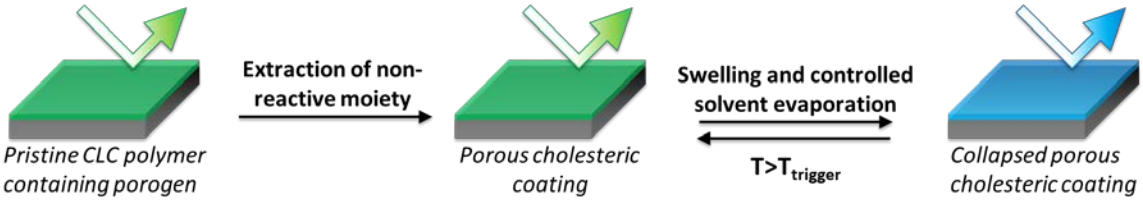

Figure 3, Scheme of shape-memory cold-programming on a photonic coating.

Hot programming of photonic polymer structure

A temperature sensor based on hot embossing of semi-interpenetrated (semi IPN) CLC polymer coatings is proposed. Following the same strategy as in (Figure 4), the CLC polymer coating is formed with a reactive CLC mixture containing a non-reactive compound which acts as a porogen after its extraction. The CLC porous polymer coating is further filled with an acrylate-based monomer to form a semi-IPN CLC polymer coating after polymerization of the monomer. The semi-IPN CLC polymer coating can be embossed at high temperature to generate a temporary and stable color-shift at room temperature which can be further recovered upon increasing the temperature above the glass transition temperature (T_g) of the polymer system. The design of a semi-IPN CLC network enables further control of the T_g and recovery rate.

PRIME has received Funding from the European Union's Horizon 2020 research and innovation programme under Grant Agreement No. 829010

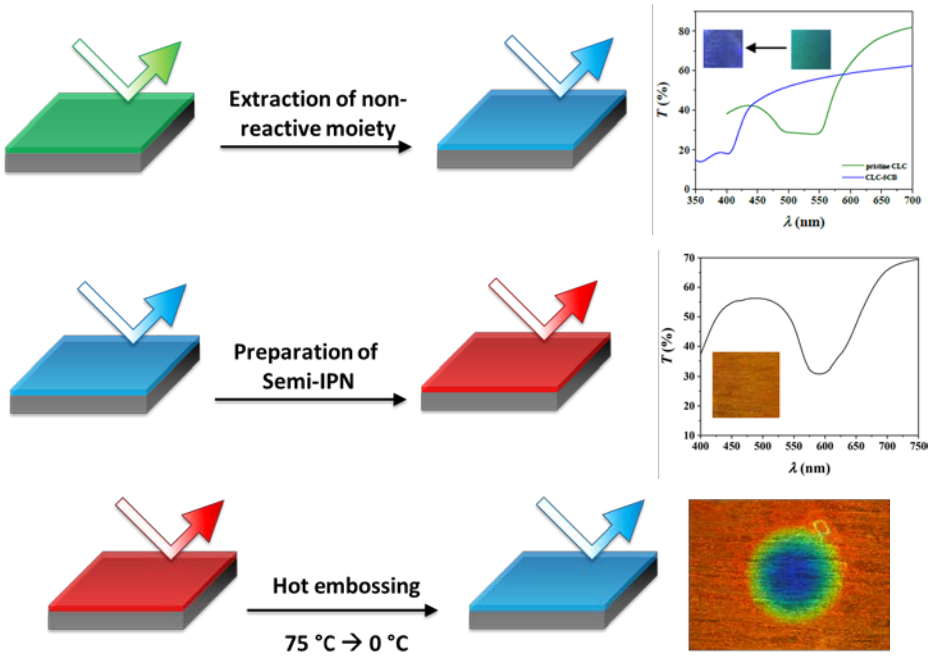

Figure 4, Scheme of shape-memory hot-programming steps on a photonic coating including Ultraviolet-visible spectroscopy (UV-Vis) graphics and a polarized optical microscopy (POM) image of the coating after programming.

Non-crosslinked photonic polymer structure (NCPPS)

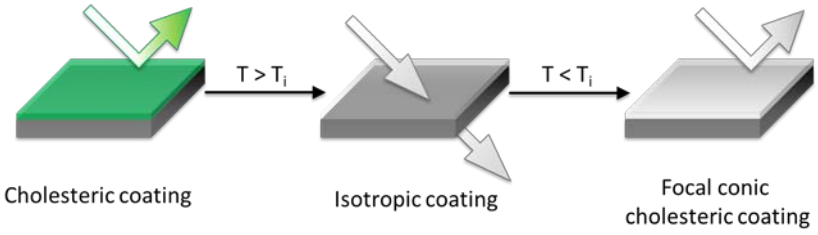

Figure 5, Scheme of optical transition on non-crosslinked photonic coatings upon temperature increase.

An optical sensor based on a non-crosslinked CLC polymer coating is proposed. The use of CLC monomers with a single acrylate functional group to form long non-crosslinked polymer chains after polymerization leads to a solid and stable polymer coating at room temperature due to the formation of hydrogen bonds between the chains. The non-crosslinked CLC polymer coating preserves the optical properties at room temperature and becomes transparent at a temperature above the isotropization temperature (T_{iso}) to eventually reach a whitish coloration (scattering state) after cooling back to room temperature due to a focal conic ordering of the CLCs (Figure 5).

PRIME has received Funding from the European Union's Horizon 2020 research and innovation programme under Grant Agreement No. 829010

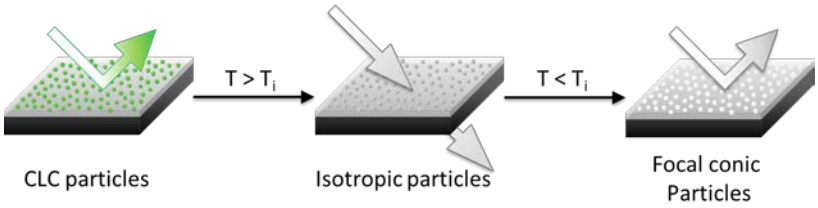

Figure 6, Scheme of optical transition on non-crosslinked photonic coatings upon temperature increase.

An optical sensor based on non-crosslinked CLC polymer particles which are dispersed in a transparent binder to form a photonic coating is also proposed. The sensing mechanism is the same as the previous optical sensor (Figure 6). The CLC particles undergo an optical transition from color-to-transparent-to-whitish upon increasing the temperature above T_{iso}. The main advantage is the possibility to design the binder to easily adapt the coating to the microfluidics requirements.

5 RESULTS

5.1 Jettable CLC thermal transducer

5.1.1 Design

Initially, a photonic polymer structure consisting of a CLC porous polymer network that can be programmed at room temperature by solvent evaporation leading to a temporary and stable optical change was proposed[34]. However, solvent-induced programming at room temperature is only possible when using inverse opals photonic structures. CLC polymer networks immediately collapse after extraction of a non-reactive compound and cannot be programmed by controlled solvent evaporation.

Next, a photonic polymer structure consisting of a semi-interpenetrated (IPN) cholesteric liquid crystalline (CLC) polymer network was considered to fabricate the irreversible optical sensor. The semi-IPN CLC network is fabricated from a CLC polymer film which is swollen with poly(benzyl acrylate) (BA) at a temperature above T_g of the film to form a semi-IPN CLC network[35] (Figure 7). The semi-IPN CLC network exhibits a broad T_g that can be exploited to fabricate an irreversible thermal sensor via shape-memory hot-programming. The film can be compressed at a temperature higher than T_g, leading to a blue-shift of the reflected color, and further stabilized at room temperature by freezing the mobility of the polymer chains below T_g. The blue-shift is originated by the compression of the cholesteric helical structure, which is responsible for the reflected color following the Bragg's law, where the reflected wavelength (ʎ) is proportional to the pitch. The original reflected color is recovered upon heating above T_g, as the polymer chains gain mobility and recover their original shape (Figure 7b). Therefore, the color-shift or optical indication depends on the T_g of the semi-IPN CLC network, which can be adjusted by changing the CLC monomers mixture and/or the interpenetrating polymer. This method enables the fabrication of irreversible optical sensors. Nonetheless, the requirement of a hot-programming thermo-mechanical process limits its application in miniaturized, compact microfluidics devices.

PRIME has received Funding from the European Union's Horizon 2020 research and innovation programme under Grant Agreement No. 829010

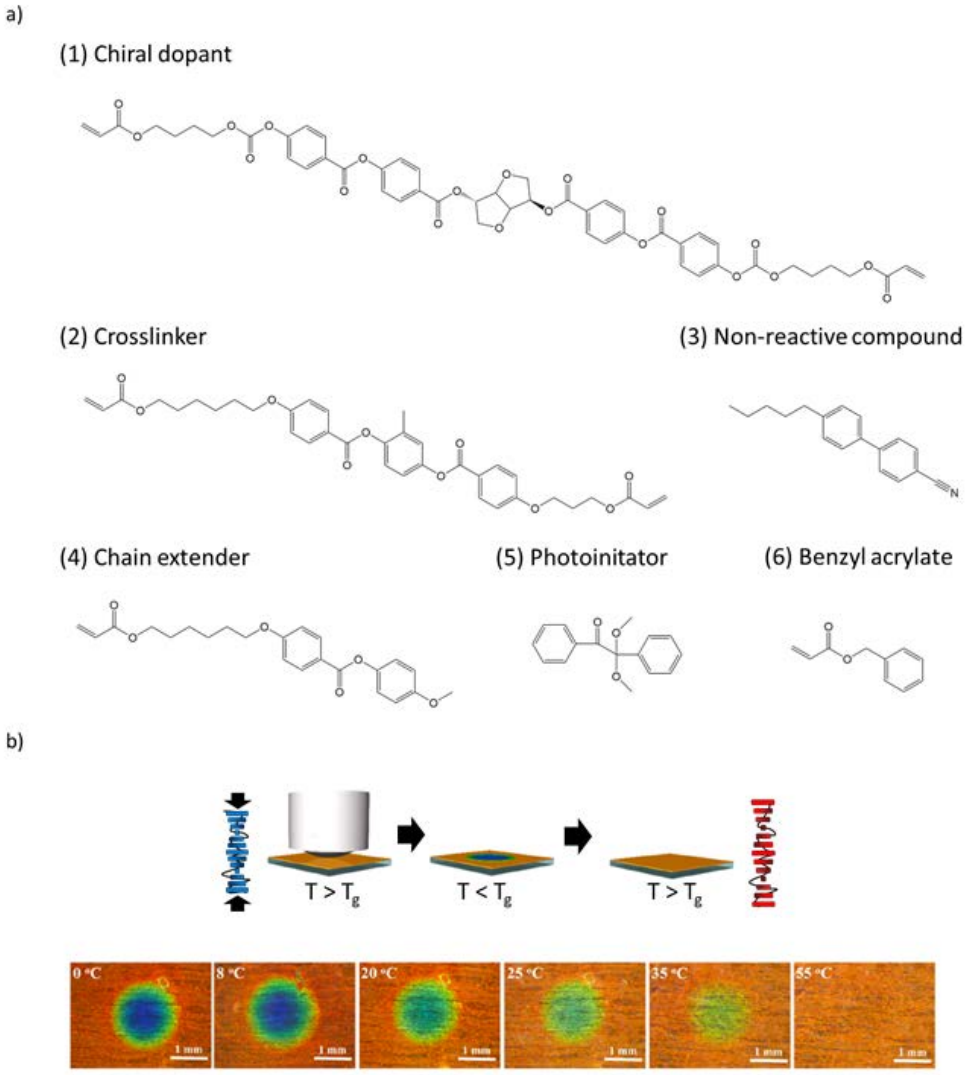

Figure 7, a) CLC monomers mixture, b) scheme of the hot-programming process and recovery including POM images of the coating.

NCPPS are better candidates as the optical response relies on a thermal phase transition and no external programming is required. The NCPPS was fabricated with a reactive CLC monomers mixture containing a chiral molecule (1), a chain extender (2), hydrogen-bonding molecules (3,4) to form dynamic crosslinks and a photoinitiator (7). All molecules have a single acrylate functional group to form a non-crosslinked network after photopolymerization of the acrylate groups[36] (Figure 8).

LC monomers having both a carboxylic acid group and an acrylate group are proposed as anchors for binding the sensing antibodies to the polymer network at the surface of the optical sensor. Such compounds are incorporated into the CLC ink and anchored to the network during photopolymerization of the acrylate groups. These compounds are expected to not disturb the alignment of the photonic structure.

PRIME has received Funding from the European Union's Horizon 2020 research and innovation programme under Grant Agreement No. 829010

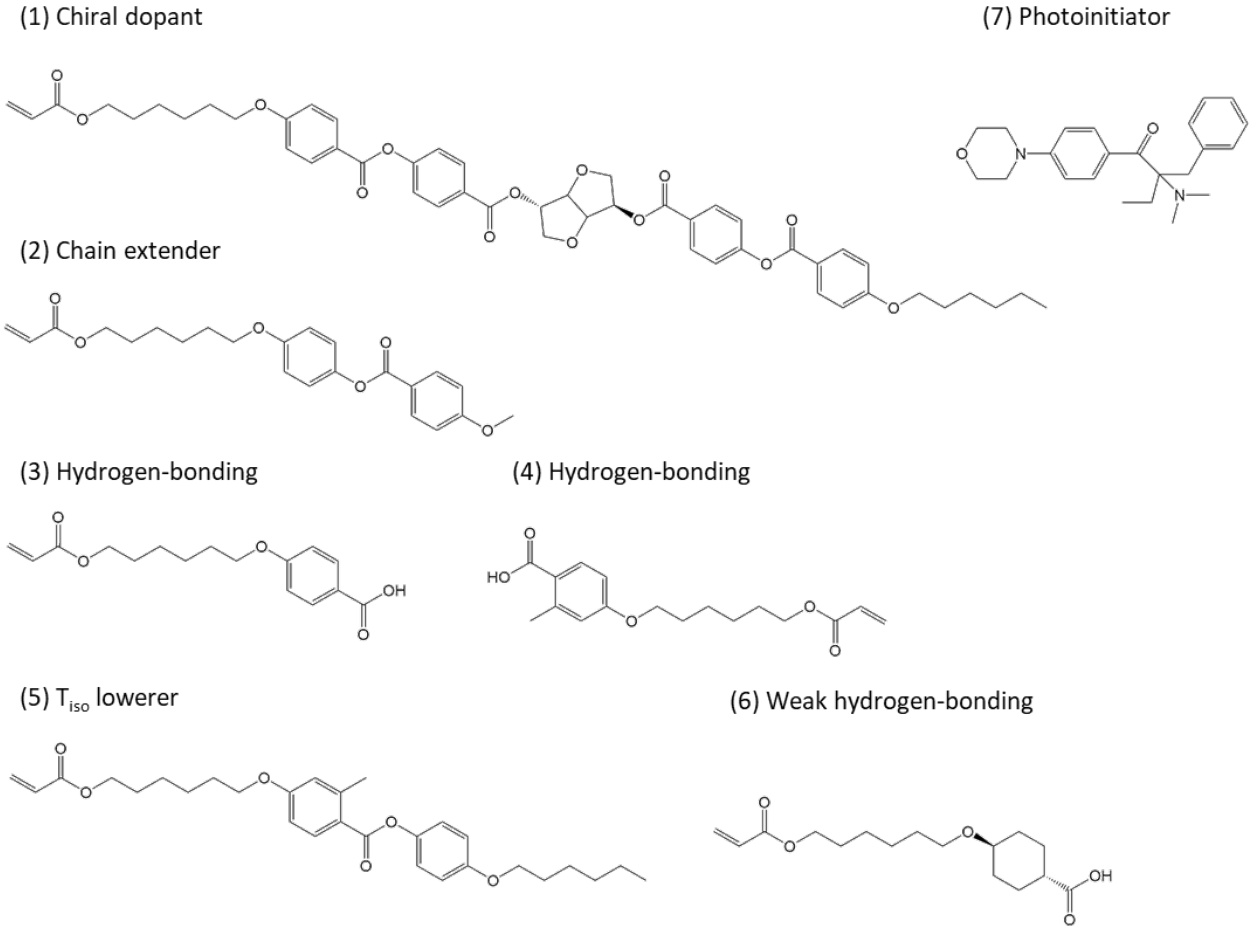

Figure 8, Chemical structures of the CLC monomers mixture used to fabricate the NCPPS.

The photonic structure exhibits an irreversible transition from cholesteric (color state) to isotropic (transparent state) to focal conic (scattering state) upon heating above T_{iso} of the polymer network and further cooling down to room temperature (Figure 9). The transition from cholesteric to focal conic states is the optical indication that a certain temperature was reached. This could be used to indirectly detect the presence of analytes through infra-red (IR) heating.

To realize direct printing of the NCCPS-based optical sensor on the microfluidics device, the above proposed CLC mixture was dissolved in cyclopentanone to reduce its viscosity and a small amount (0.1 wt%) of surfactant was added to achieve planar alignment of the liquid crystals (LCs) at the coating-air interface. A black biaxially stretched polyethylene terephthalate foil was chosen as the substrate to enhance the color appearance and to provide planar alignment of the LCs. After printing, the solvent was evaporated, and the print was cooled down to below T_{iso} to develop the cholesteric photonic structure. Finally, the photonic structure was photopolymerized into a photonic polymer network upon ultraviolet (UV) light exposure.

PRIME has received Funding from the European Union's Horizon 2020 research and innovation programme under Grant Agreement No. 829010

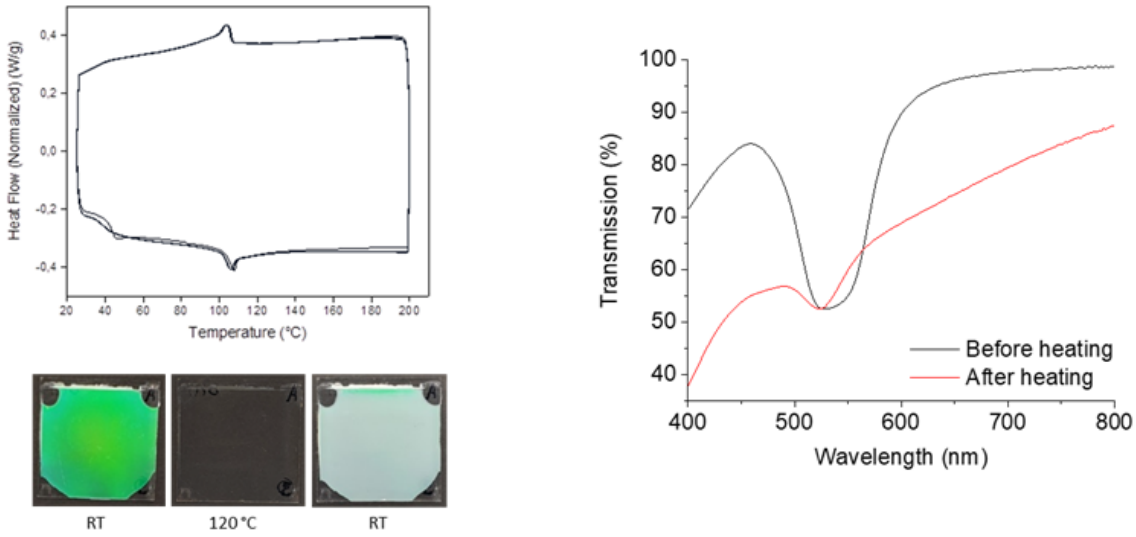

Figure 9, Differential scanning calorimetry (DSC) of the NCPPS and transmission change of coating upon thermal treatment.

The CLC mixture was optimized to decrease T_{iso} of the photonic polymer network down to different operational temperatures (for example, around 65°C, Figure 10). Compound (5) was added as it has a low T_{iso} itself and compounds (3) and (4) were replaced by compound (6) to obtain a lower hydrogen bonding strength in comparison with the previous system[37] (Figure 8).

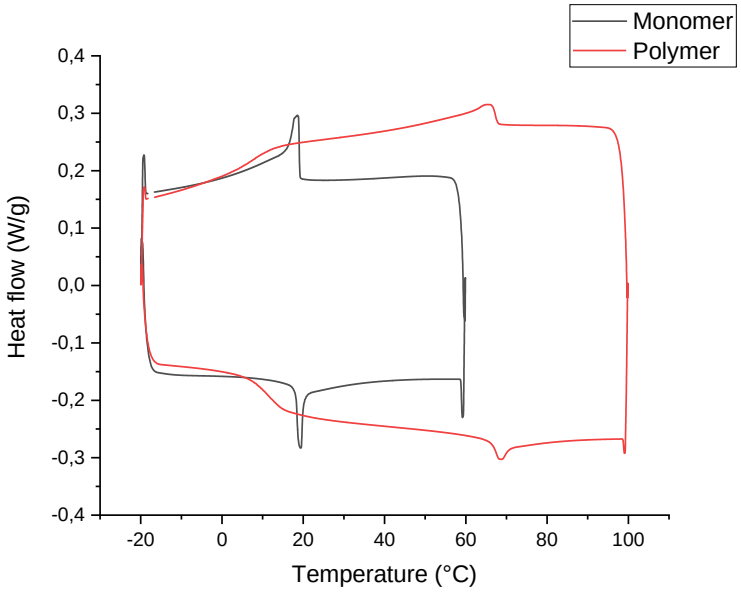

Figure 10, DSC trace of optimized monomer formulation (black) and polymer (red).

PRIME has received Funding from the European Union's Horizon 2020 research and innovation programme under Grant Agreement No. 829010

Adjusting the proportions of compounds 3 and 4, the operational temperature or T_{iso} of the photonic structure was decreased from 100°C to 65°C. Moreover, the initial color state of the photonic structure is easily modified from blue to red by decreasing the proportion of the chiral dopant (1). It was noticed that the color of the coatings in the monomeric state varied with the polymerization temperature. This was verified by measuring the transmission of an unpolymerized coating as a function of temperature (Figure 11). This property can be used to precisely tune the color towards the aimed color.

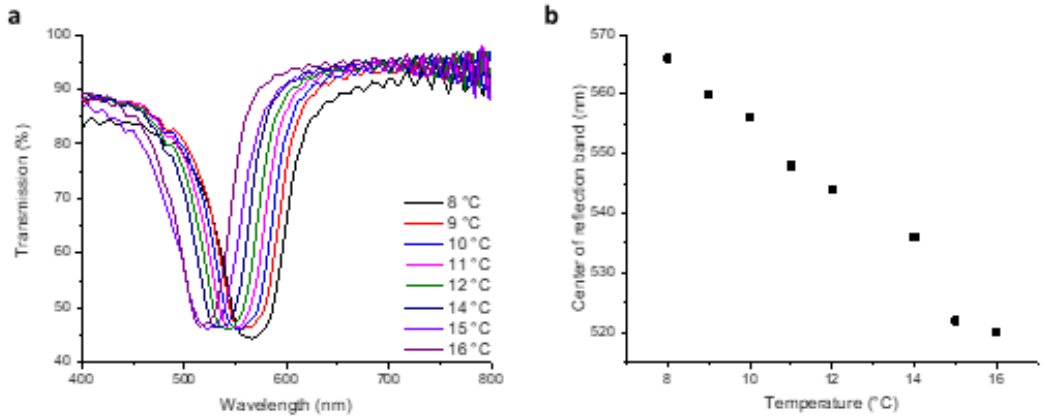

Figure 11, a) Transmission spectra and b) reflection peak as a function of temperature.

5.1.2 Multi-temperature sensing

An easily readable temperature sensor was designed to go from green to red with increasing operational temperatures from 66°C to 97 °C (Figure 12 and formulations in Table 1). CLC mixtures having different concentrations of chiral dopant and proportions of compounds 3 and 4 were inkjet printed on the black foil, cooled down and photopolymerized for 2 minutes with high intensity UV light. The polymerized coatings show a bright green, orange and red color upon normal (perpendicular) viewing.

Table 1, Chemical composition of the different formulations of study in wt.% (monomers nomenclature from Figure 8).

Monomers	***Green coating***	***Orange coating***	***Red coating***
(1)	3.1	2.9	2.7
(2)	62.5	69.1	77.3
(5)	12.6	10.2	7.2
(6)	21.0	17.0	12.0
(7)	0.8	0.8	0.8

PRIME has received Funding from the European Union's Horizon 2020 research and innovation programme under Grant Agreement No. 829010

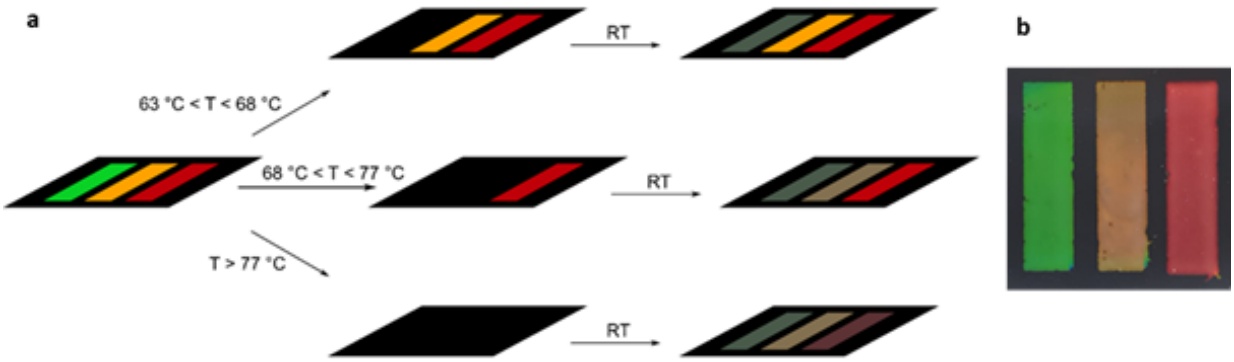

Figure 12, a) Schematic representation of the temperature sensor and b) picture of a printed sample upon normal (perpendicular) viewing.

The reflection was investigated as a function of temperature for each of the different colored coatings. Figure 13a shows an abrupt decrease of the reflection peak when the temperature reaches $T_{iso,}$ pointing out the disorder of the cholesteric structure (transparent state). After cooling down to room temperature, the reflection peak is not recovered (Figure 13b, dashed lines) and the photonic coatings exhibit a whitish color attributed to scattering caused by a focal conic re-organization of the cholesteric structure (Figure 13c). Above T_{iso}, the un-crosslinked polymer chains gain mobility and can freely flow adopting a different internal configuration, thus impeding the further recovery of the initial cholesteric alignment but leading to a random organization of the cholesteric domains.

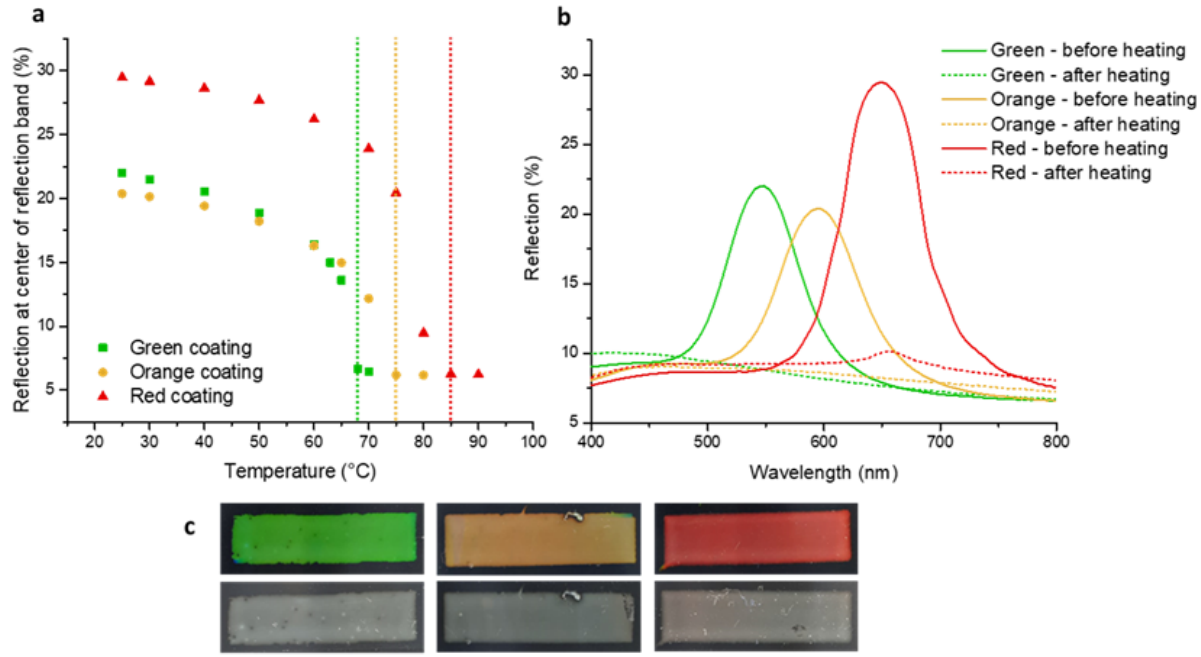

Figure 13, a) Reflection (%) at the reflection peak for each of the different colored coatings. Green: 548 nm, orange: 596 nm and red: 650 nm, b) reflection spectra before and after heating and c) pictures of the coatings before (upper row) and after (lower row) heating.

PRIME has received Funding from the European Union's Horizon 2020 research and innovation programme under Grant Agreement No. 829010

Finally, the sensors were tested underwater to investigate the response in conditions like those in the microfluidics device (Figure 14). The coatings showed to be stable and experienced the same optical transition than on-air experiments upon temperature increase.

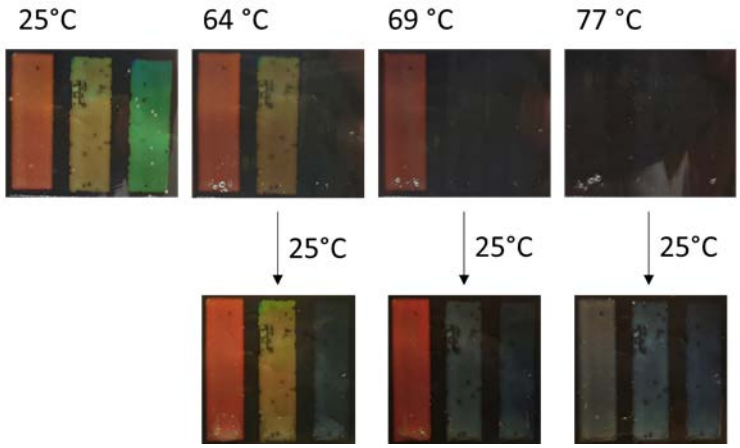

Figure 14 Photographs of sensors heated above T_{iso}(top) and cooled down (bottom) in an aqueous environment.

5.1.3 Time-temperature Dependence

The optical sensors exhibit time-temperature dependence when subjected to isothermal steps at temperatures close to the isotropization temperature. The color progressively redshifts with time under isothermal conditions (Figure 15) at a temperature below T_{iso}. The redshift is related to the relaxation of the polymer network. During relaxation, the CLC helical structure unwinds to a less hindered and energetically favored configuration, increasing the pitch. The red-shift is combined with a loss in order when the isothermal temperature is close to T_{iso} (i.e. 64°C). This can be exploited in the fabrication of time-temperature integrators.

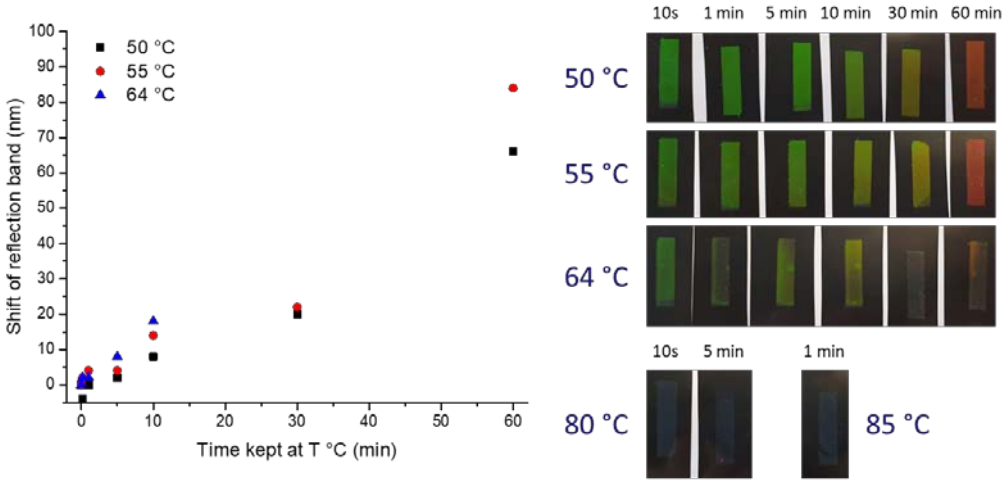

Figure 15, a) Reflection shift as a function of the time in a green coating sample subjected to different isothermal processes and b) pictures of the sample.

PRIME has received Funding from the European Union's Horizon 2020 research and innovation programme under Grant Agreement No. 829010

5.2 CLC thermal transducer particles

As mentioned above, cholesteric layers usually require alignment layers to show optimum optical reflective properties. The incorporation of these alignment layers introduces new steps in the fabrication process complicating production. An alternative approach to eliminate the need for these alignment layers in the optical sensor is here proposed.

The CLC ink can be used to fabricate photonic polymer particles as micron-sized optical indicators by suspension polymerization (Figure 16). Droplets of the CLC ink are formed at T_{iso} in a water-based medium with polyvinyl alcohol (PVA) as a surfactant to further induce the cholesteric alignment. The emulsion is cooled down to 10°C from the cholesteric phase. Afterward, the droplets are photopolymerized into polymer particles upon exposure to UV light. The CLC particles are washed and dried to obtain a fine powder.

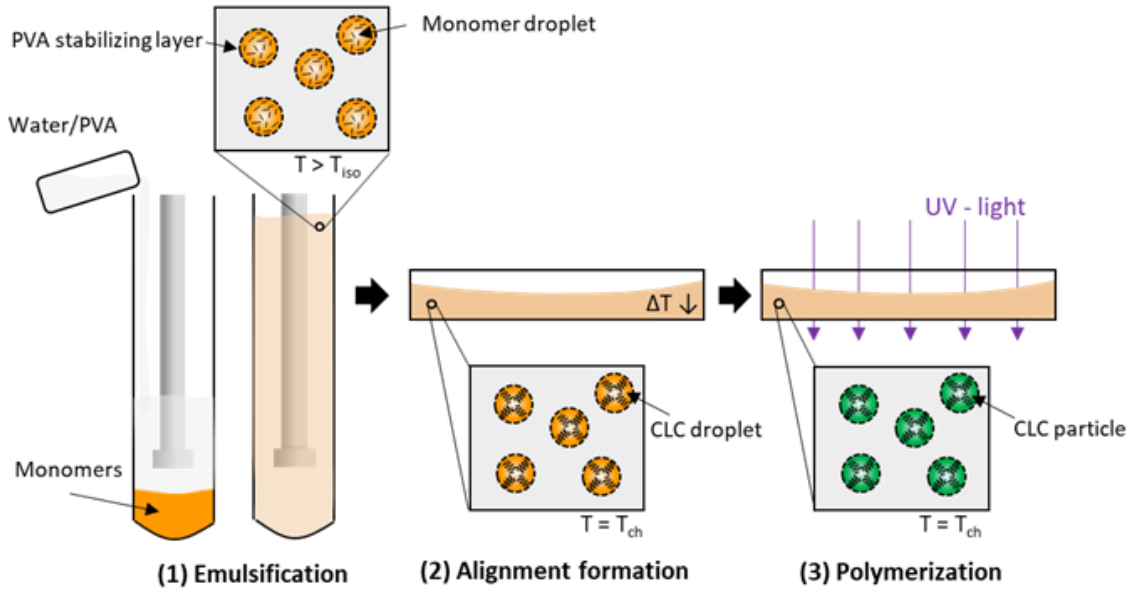

Figure 16, Scheme of the different steps for the synthesis of the cholesteric particles.

The CLC particles can be dispersed in a liquid binder to form precursor materials that can be applied on the microfluidic device to form a particles-based polymer film after photopolymerization of the binder. This method enables a free design of the binder to facilitate the binding of analytes to the surface without interfering with the optical performance of the sensor. Early experiments on a water/PVA based coating formed on a glass plate (Figure 17a), demonstrate that the particles undergo the same optical transition as observed for the NCPPS when heated above the isotropization temperature (Figure 17b).

PRIME has received Funding from the European Union's Horizon 2020 research and innovation programme under Grant Agreement No. 829010

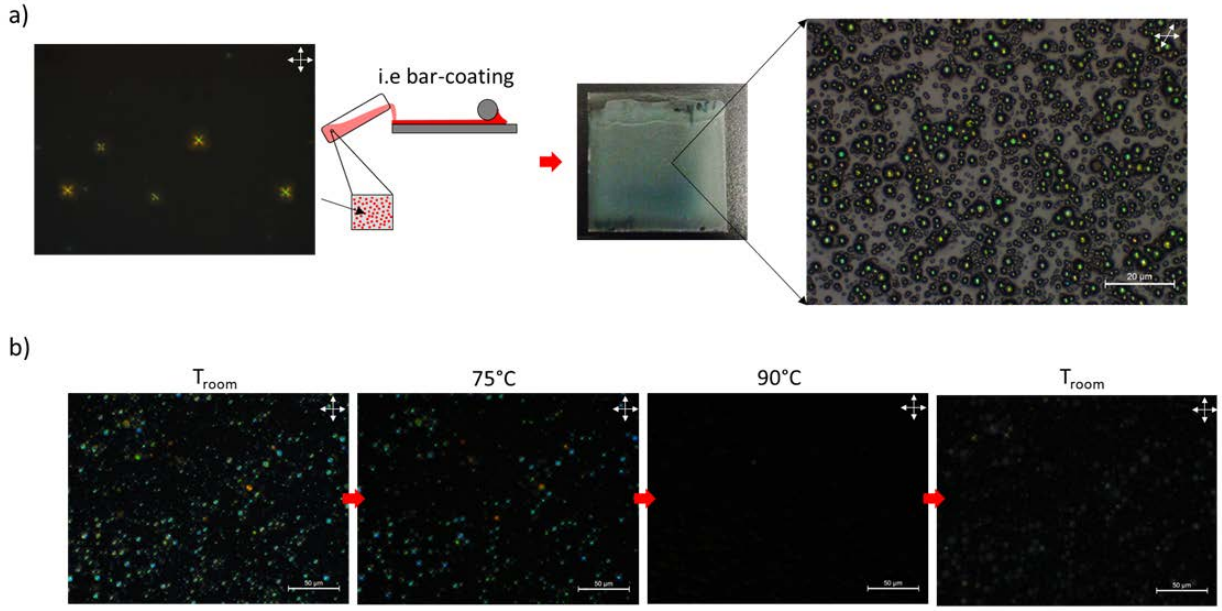

Figure 17, Coating of a water/PVA-based ink of cholesteric particles prepared on a glass plate by bar-coating and the response of the particles optical performance to a thermal process.

5.3 Biofunctionalization and Sensing using CLCs

5.3.1 Gold Nanoprisms Synthesis

Three types of AuNPRs with different plasmon have been synthesized. The AuNPRs are pegylated to make them stable and easily coordinated by the carboxyl on their surface. After the purification, their concentrations are obtained by ICP and the average edge length was studied using Scanning Electron microscopy (SEM), obtaining 277 ± 36 nm, 221 ± 21 nm, 199 ± 29 nm (Figure 18) corresponding the localized surface plasmon resonance (LSRP) characterized by UV-Vis spectroscopy with NIR bands centered at 1230, 1026 and 846 nm respectively. This optical property allows AuNPrs to convert light energy into heat by the photothermal effect. To evaluate the heating capability, the same concentration (15 µg/mL) of these three types of NPRs were irradiated with a 1064 nm laser with a power of 1224 mW, obtaining the heating curves (heating and cooling cycle) by a thermal image with an infrared camera. From these thermal signals, the calculation of the photothermal conversion efficiency (η) of each AuNPrs was carried out showing the larger NPRs the highest photothermic efficiency and therefore these were the ones selected to use.

5.3.2 ThermoELISA Sandwich Immunoassay

The concentration of immobilized capture antibody and the detection biotinylated antibody were optimized, for each cancer marker, using the optimized colorimetric ELISA protocol to validate the sandwich antibodies and to know the best limits of detection and quantification of the method, to compare these with the obtained in thermoELISA. First, different ELISAs were carried out, to evaluate the optimal concentration of capture antibody (12 µg/mL anti-CEA capture Ab, 5 µg/mL

PRIME has received Funding from the European Union's Horizon 2020 research and innovation programme under Grant Agreement No. 829010

anti-hVEGF capture Ab and 5 µg/mL anti-CA199 capture Ab) using a constant concentration of each detection antibody. Secondly, the detection biotinylated antibody concentration was optimized (1 µg/mL Anti-CEA detection Ab biotin-labelled, 0.2 µg/mL anti-hVEGF detection Ab biotin-labelled and 2 µg/mL anti-CA199 detection Ab biotin-labelled). The evaluation of the newly developed and optimized methodology was carried out repeating the thermoELISA analysis three times for each cancer marker. In the case of the CEA, the colorimetric ELISA does not reach the necessary levels of quantification that thermoELISA can be reached, with which we can even reach levels of detection of 0.91 ng/mL. For de detection of CA19.9, the limits of quantification for both methods are very similar and are already well below the concentration needed to detect (Figure 18).

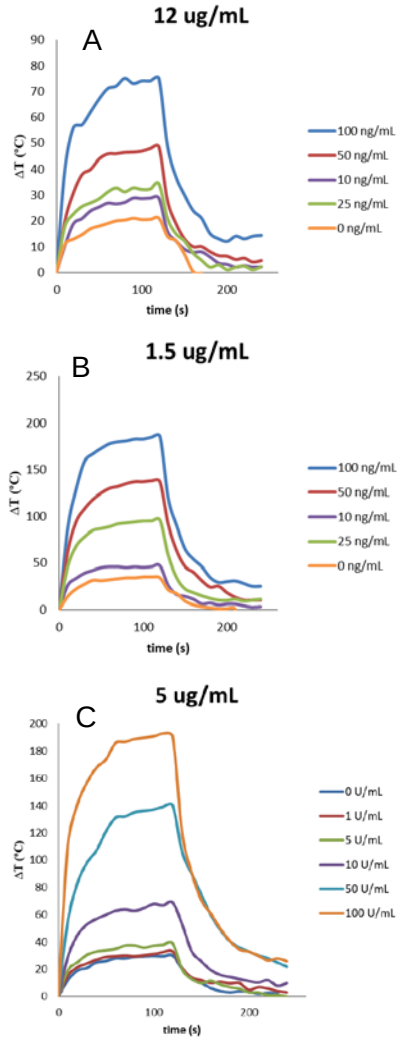

CEA	
[Ab_det]	Sensitivity
2 ug/mL	42.49
6 ug/mL	56.88
10 ug/mL	60.37
12 ug/mL	69.67

VEGF	
[Ab_det]	Sensitivity
0.5 ug/mL	318.9
1.5 ug/mL	274.02
2.5 ug/mL	272.22

CA19.9	
[Ab_det]	Sensitivity
5 ug/mL	321.04
10 ug/mL	239.93
15 ug/mL	230.63

Figure 18, ThermoELISA signals for the optimized concentration of biotinylated detection antibody and the sensitivities obtained in each case. A-Results obtained for CEA. B-Results obtained for VEGF.C-Results obtained for CA19.9

Finally, for VEGF, the thermoELISA improves four times the quantification limit of the colorimetric ELISA but none can quantify the low concentration of active disease (Table 2). However, the detection limit for the thermoELISA is very close to the value for the active disease improving the

PRIME has received Funding from the European Union's Horizon 2020 research and innovation programme under Grant Agreement No. 829010

one obtained for colorimetric ELISA. Thus, the thermoELISA developed greatly increases the sensitivity with respect to the classic colorimetric ELISA, decreases the limits of detection and quantification with a low RSD, highlighting the transduction capacity of these nanomaterials in biological assays, as well as their possibilities in the development of biosensors.

Table 2, Analytical data comparing the classic colorimetric ELISA and ThermoELISA optimized.

Analyte	Range (ng/mL)	Sensitivity	LOD(ng/mL)	LOQ(ng/mL)	%RSD
CEA					
Colorimetric ELISA	18,58-100	1,02	5,57	18,58	20,8
ThermoELISA	3,03-100	74,74	0,91	3,03	11,58
CA19.9					
Colorimetric ELISA	0,42-50	6.23	0,13	0,42	8,37
ThermoELISA	0,63-50	520,62	0,19	0,63	9,22
VEGF					
Colorimetric ELISA	4,76-100	3,11	1,42	4,76	12,07
ThermoELISA	1,88-100	258,90	0,56	1,88	10,53

5.3.3 CLC polymer compatibility with the sample treatment

One of the aims of the work was to prove that the color and the structure of the CLC polymer remained stable along with the thermoELISA protocol. Especially, during the activation step (incubation with EDC-NHS) and the binding step with the capture antibody, which are the most critical points. Two different NCCPS-based materials, Ref +23 and Ref 15/25, supplied by TU/e with transition temperatures at 66 and 114 ºC respectively have been employed. In order to work in a 24 well plates, the CLC polymers were cut in a small square of 1 cm^2 using a diamond marking pencil.

Three replicates of both samples (Ref +23 and Ref 15/25) were subjected to the entire activation step and the capture antibody step. One replicate of each mixture of CLC polymer was subjected only to the activation step without drying. Additionally, one replicate of each mixture of CLC polymer was subjected to the activation step following by a drying step. Finally, only MES buffer was added to both Ref +23 and Ref 15/25 so these samples were used as a negative control. Table 3 comprises the RGBs measurements at the beginning and the end of the protocol.

Table 3, Comparison between RGBs obtained at the beginning and at the end of the protocol.

	RGBs			
	Ref+23		Ref. 15/25	
Sample Name	**Initial**	**Final**	**Initial**	**Final**
Positive control 1	202,218,176	190,181,158	187,186,175	190,190,177
Positive control 2	190,170,156	177,165,141	194,177,160	190,178,150
Positive control 3	199,197,185	175,163,139	190,163,148	178,149,130
Activation+dry	181,179,168	200,200,184	162,153,115	188,177,145
Activation	198,189,171	195,190,170	185,167,142	197,184,158
Negative control	186,184,173	191,191,175	181,176,147	181,180,166

The RGBs of the CLC crystals were measured using a mobile camera. These RGB coordinates were converted to CIELAB coordinates using a Color Space Converter provided by ImageJ software.[38] The CIELAB color space is explained by using three coordinates (L*, a* and b*), each

PRIME has received Funding from the European Union's Horizon 2020 research and innovation programme under Grant Agreement No. 829010

one provides different information: color model: L* = Lightness (also referred to as luminance); the lightness or darkness of a color a* = red to green (+a = redder, -a = greener) b* = yellow to blue (+b = yellower, -b = bluer). Total color differences are measured by $\Delta E = ((\Delta L^*)^2 + ((\Delta a^*)^2 + ((\Delta b^*)^2)^{1/2}$. No large differences were observed regarding the ΔE parameter for both samples during the different sample treatments, especially in Ref 15/25 which remained stable in all the cases. More total color differences were observed in Ref +23 were positive controls exhibited the larger ones. Particularly, in ΔL^* parameter which indicated a loss of brightness but that did not mean a critical change in the structure of the CLC polymer, so it allowed keeping on binding the rest of thermoELISA sandwich.

5.3.4 CLC polymer ThermoELISA results

ThermoELISA protocol was carried out for both samples (Ref +23 and 15/25). There were different trials of experiments, a scheme of them could be found in Figure 19.

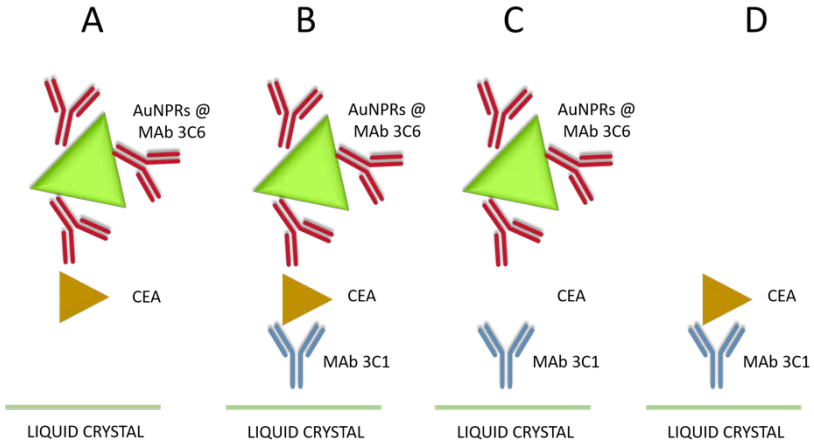

Figure 19, Different trials carried out along the experiment. Different letters correspond to different trials carried out along the experiment A: without capture antibody (MAb3C1), B: positive control (completed sandwich), C: without antigen and finally D: without nanoparticle

PRIME has received Funding from the European Union's Horizon 2020 research and innovation programme under Grant Agreement No. 829010

Table 4 comprises the RGBs measurements at the beginning and at the end of the protocol.

Table 4, RGBs obtained from CLC polymers at the beginning and at the end of the experiment.

RGBs						
	Ref+23			Ref. 15/25		
Sample Name	**Initial**			**Initial**		
	1	**2**	**3**	**1**	**2**	**3**
A	230,240,219	171,242,175	177,219,133	231,255,211	211,246,162	205,244,193
B	158,216,175	141,255,155	127,245,156	212,209,191	226,235,205	184,237,165
C	198,248,205	134,238,180	178,197,185	221,252,205	197,245,180	241,254,222
D	223,224,188	134,238,180	188,217,195	196,209,167	199,208,156	216,254,190
Sample Name	Final			Final		
	1	2	3	1	2	3
A	146,150,127	96,194,94	92,188,117	205,180,17	159,127,107	126,116,99
B	80,142,127	77,181,88	138,185,132	184,181,171	157,143,124	191,170,158
C	65,186,97	19,164,52	100,87,98	181,183,145	127,171,107	143,123,122
D	96,116,104	35,42,40	105,119,107	206,183,179	141,141,104	135,127,123

Slight differences in color in both references could be appreciated by comparing the appearance at the beginning and at the end of the protocol. ΔE parameter exhibited values between 24 and 79 for Ref +23, and between 11 and 72 in the case of Ref 15/25.

In general, they all lose brightness due to ΔL parameter was negative in all cases. The same happened with Δa* and Δb* parameters, as a consequence it could be said that the crystals became greener and bluer. The appearance of the CLC polymers is shown in Figure 20.

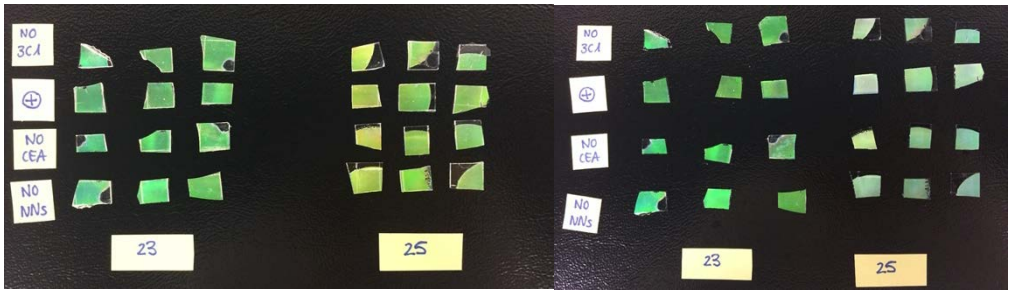

Figure 20, Differences of temperature after irradiating both sides of the non-CLC polymer

Regarding the temperature profiles obtained after laser irradiation, it could be said that the functionalization worked properly in both references for the positive controls (B trials). Ref +23, exhibited more ΔT than Ref 15/25 but both were larger than the rest of the trials (A, C and D), as expected because the positive controls were the only trials that have the sandwich completed. The results obtained are shown in Table 5.

PRIME has received Funding from the European Union's Horizon 2020 research and innovation programme under Grant Agreement No. 829010

Table 5, Temperature differences obtained after laser irradiation

	ΔT (ºC)					
SAMPLE NAME	**Ref +23**			**Ref 15/25**		
	1	**2**	**3**	**1**	**2**	**3**
A	1,2	0,4	0,1	0,3	0,3	0,5
B	50,1	28,0	48,4	13,6	11,6	32,3
C	3,3	1,2	2,4	8,4	11,3	12,2
D	0,5	0,6	0,9	0,7	1,2	0,9

5.3.5 Optimizing blocking agent for AuNPRs

One important step along the bioconjugation protocol is to block properly the nanoparticle after adding the detection antibody. It is necessary to block the rest of the carboxyl groups present on the surface of the nanoparticle to avoid possible nonspecific interactions or adsorption with other proteins or components of the sample. There are numerous blocking agents but in this case two blocking agents were chosen, such as serum albumin protein (BSA) and a 7500 Da polyethylene glycol (PEG).

5.3.6 BSA

BSA agent exhibited reproducible behavior between the three replicates but less temperature increase only 4,5 ºC comparing to the initial temperature. The obtained results are shown in Figure 21.

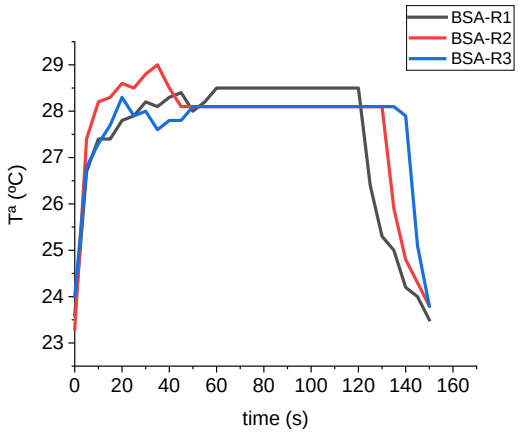

Figure 21, Temperature profile achieved after blocking the nanoparticle with BSA agent

5.3.7 PEG

PEG agent exhibited an important temperature rise in all the samples, especially in the case of replicate 2 more than 40 ºC, as it is shown in Figure 22 These findings indicate that PEG acts better as a blocking agent than BSA. BSA is a large molecule that can avoid the binding with the antigen in the sample.

PRIME has received Funding from the European Union's Horizon 2020 research and innovation programme under Grant Agreement No. 829010

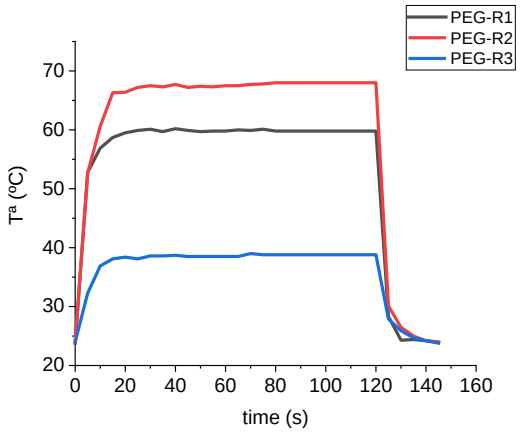

Figure 22, Temperature profile achieved after blocking the nanoparticle with PEG agent.

Highlighting the fact that it is only one side functionalized, several experiments were done in order to demonstrate if there are any differences between the different sides of the non-CLC polymers when they are irradiated with the laser. It is important to remark that the functionalized side is side 1 and the no functionalized side is side 2. As it is shown in Figure 23. Temperature is measured using an IR camera placed at the bottom of the scheme below the sample.

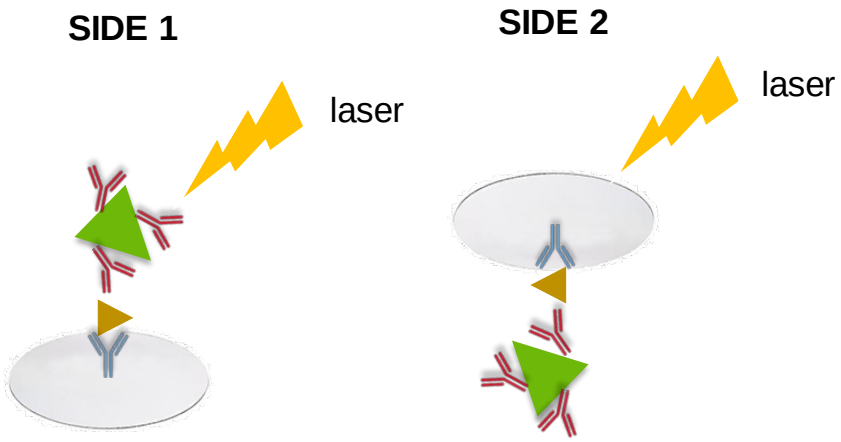

Figure 23, Scheme of the two sides of a non CLC polymer. Temperature is measured from the bottom in the scheme by using an IR camera

The results can be found in Table 6. In the case of blank samples (consisting of a non-CLC polymer without subjecting to any functionalization) the same temperature was observed irradiating the functionalized side of the non-cholesteric crystal and by the opposite side. The same happened also in BSA samples. In PEG samples it was noticed a large difference between both sides, due to the more temperature increase the more chance to see this phenomenon. Side 2 exhibited more temperature rise in PEG samples despite the fact not being the functionalized side, but it could be explained as the heat dissipation process because the non-irradiated side which is the functionalized side is closer to de IR camera.

PRIME has received Funding from the European Union's Horizon 2020 research and innovation programme under Grant Agreement No. 829010

Table 6, Differences of temperature after irradiating both sides of the non-CLC polymer

ΔT (ºC)						
REPLICATE	**Blank**		**PEG**		**BSA**	
	Side 1	**Side 2**	**Side 1**	**Side 2**	**Side 1**	**Side 2**
1	0,0	0,4	11,7	35,4	2,5	44,7
2	0,2	0,4	36,5	44,0	3,6	4,9
3	0,9	1,6	6,7	15,3	6,0	3,8
mean	**0,4**	**0,8**	**18,3**	**31,6**	**4,0**	**3,8**

PRIME has received Funding from the European Union's Horizon 2020 research and innovation programme under Grant Agreement No. 829010

6 CONCLUSIONS

We developed a jettable ink formulation to print thermo-responsive optical coatings with tunable color and detection temperature between ~65 °C and ~85 °C. A multi-temperature optical sensor was inkjet-printed using the developed ink and showed high stability underwater conditions. The printed coatings also showed a gradual red-shift when exposed to elevated temperatures below the isotropization temperature. This could be exploited for the development of a time-temperature integrating (TTI) sensor where the color shift represents the time at which the sensor was held at a certain temperature. Furthermore, non-crosslinked CLC polymer particles were synthesized to enable a free design of a functional binder for the ink. Preliminary results using a water-based ink showed that the particles respond to temperature like the inkjet-printed sensors. However, the initial optical state of the sensor was already scattering due to a RI mismatch between the particles and the binder, and surface roughness.

Regarding the biosensor construction, firstly, the ELISA sandwich proposed for building up the biosensor worked properly with the first CLC polymer in terms we were able to see an increase of temperature after irradiating with the laser. Despite these observations, we notice a bit change in the color in both samples of CLC polymer after applying the whole protocol. Secondly, blocking agent PEG exhibited the best behavior as a blocking agent. Blocking properly the nanoparticle after adding the capture antibody is an important step of the bioconjugation protocol. Finally, a similar temperature increase was detected irradiating both the functionalized side and the non-functionalized side, this finding opens new possibilities of building up different biosensor configurations.

7 OPEN POINTS AND OUTLOOK

The printed optical coatings are not yet optimized for the use in thermoELISA bioassays. For this, the detection response should be at a lower temperature and faster. Furthermore, the density of the anchors on the surface for the bio-functionalization varies between different formulations, leading to low reproducibility. Therefore, a “standard layer” with constant anchor-density is preferred. This can potentially be achieved using a PDMS layer between the CLC layer and the bio-functionalized layer. The possibility of using a PDMS layer will ease the optimization of the construction of the biosensor. From this point, the next challenge will be to build up the ELISA sandwich over this layer and see its behavior after irradiating the whole structure with the laser.

Another solution could be presented by using CLC particles. The binder can be functionalized with a known number of anchoring groups. During the next reporting period, efforts will be made optimizing both the particles and the binder to be compatible with DIW and reducing scattering in the initial state. Furthermore, anchoring groups will be introduced to the binder to facilitate the bio-functionalization. In the same way, the working pH and incubation time will be optimized for each capture antibody to find a more suitable environment for doing this binding.

Furthermore, efforts will be made modeling the TTI response and the development of a TTI sensor and at the same time, more attention will be paid to achieve a more efficient bioconjugate.

PRIME has received Funding from the European Union’s Horizon 2020 research and innovation programme under Grant Agreement No. 829010

8 REFERENCES

1. Keighley, M. R. B. Gastrointestinal cancers in Europe. *Aliment. Pharmacol. Ther. Suppl.* **18**, 7–30 (2003).
2. Baniak, N., Senger, J. L., Ahmed, S., Kanthan, S. C. & Kanthan, R. Gastric biomarkers: A global review. *World J. Surg. Oncol.* **14**, 1–14 (2016).
3. Dbouk, H. A., Tawil, A., Nasr, F., Kandakarjian, L. & Abou-Merhi, R. Significance of CEA and VEGF as Diagnostic Markers of Colorectal Cancer in Lebanese Patients. *Open Clin. Cancer J.* **1**, 1–5 (2007).
4. Sandblom, G., Granroth, S. & Rasmussen, I. C. TPS, CA 19-9, VEGF-A, and CEA as diagnostic and prognostic factors in patients with mass lesions in the pancreatic head. *Ups. J. Med. Sci.* **113**, 57–64 (2008).
5. Hyodo, I. *et al.* Clinical significance of plasma vascular endothelial growth factor in gastrointestinal cancer. *Eur. J. Cancer* **34**, 2041–2045 (1998).
6. Căinap, C. *et al.* Classic tumor markers in gastric cancer. Current standards and limitations. *Clujul Med.* **88**, 111–115 (2015).
7. Grodzinski, P., Silver, M. & Molnar, L. K. Nanotechnology for cancer diagnostics: Promises and challenges. *Expert Rev. Mol. Diagn.* **6**, 307–318 (2006).
8. Huang, X., Jain, P. K., El-Sayed, I. H. & El-Sayed, M. A. Gold nanoparticles: Interesting optical properties and recent applications in cancer diagnostics and therapy. *Nanomedicine* **2**, 681–693 (2007).
9. Pei, X. *et al.* Sandwich-type immunosensors and immunoassays exploiting nanostructure labels: A review. *Anal. Chim. Acta* **758**, 1–18 (2013).
10. Liu, G. & Lin, Y. Nanomaterial labels in electrochemical immunosensors and immunoassays. *Talanta* **74**, 308–317 (2007).
11. Elahi, N., Kamali, M. & Baghersad, M. H. Recent biomedical applications of gold nanoparticles: A review. *Talanta* **184**, 537–556 (2018).
12. Zeng, S. *et al.* A Review on Functionalized Gold Nanoparticles for Biosensing Applications. *Plasmonics* **6**, 491–506 (2011).
13. Maksimova, I. L. *et al.* Near-infrared laser photothermal therapy of cancer by using gold nanoparticles: Computer simulations and experiment. *Med. Laser Appl.* **22**, 199–206 (2007).
14. Riley, R. S. & Day, E. S. Gold nanoparticle-mediated photothermal therapy: applications and opportunities for multimodal cancer treatment. *Wiley Interdiscip. Rev. Nanomedicine Nanobiotechnology* **9**, (2017).
15. Pissuwan, D., Valenzuela, S. M. & Cortie, M. B. Therapeutic possibilities of plasmonically heated gold nanoparticles. *Trends Biotechnol.* **24**, 62–67 (2006).
16. Abadeer, N. S. & Murphy, C. J. Recent Progress in Cancer Thermal Therapy Using Gold Nanoparticles. *J. Phys. Chem. C* **120**, 4691–4716 (2016).
17. Baffou, G. *et al.* Thermal imaging of nanostructures by quantitative optical phase analysis. *ACS Nano* **6**, 2452–2458 (2012).

PRIME has received Funding from the European Union's Horizon 2020 research and innovation programme under Grant Agreement No. 829010

18. Elliott, A. M. *et al.* Laser-induced thermal response and characterization of nanoparticles for cancer treatment using magnetic resonance thermal imaging. *Med. Phys.* **34**, 3102–3108 (2007).

19. Qin, Z. *et al.* Significantly improved analytical sensitivity of lateral flow immunoassays by using thermal contrast. *Angew. Chemie - Int. Ed.* **51**, 4358–4361 (2012).

20. Polo, E., Del Pino, P., Pelaz, B., Grazu, V. & De La Fuente, J. M. Plasmonic-driven thermal sensing: Ultralow detection of cancer markers. *Chem. Commun.* **49**, 3676–3678 (2013).

21. Jiang, K., Smith, D. A. & Pinchuk, A. Size-dependent photothermal conversion efficiencies of plasmonically heated gold nanoparticles. *J. Phys. Chem. C* **117**, 27073–27080 (2013).

22. Alfranca, G. *et al.* Gold nanoprism-nanorod face off: Comparing the heating efficiency, cellular internalization and thermoablation capacity. *Nanomedicine* **11**, 2903–2916 (2016).

23. Chou, C. H., Chen, C. D. & Wang, C. R. C. Highly efficient, wavelength-tunable, gold nanoparticle based optothermal nanoconvertors. *J. Phys. Chem. B* **109**, 11135–11138 (2005).

24. Pelaz, B. *et al.* Tailoring the synthesis and heating ability of gold nanoprisms for bioapplications. *Langmuir* **28**, 8965–8970 (2012).

25. White, T. J., McConney, M. E. & Bunning, T. J. Dynamic color in stimuli-responsive cholesteric liquid crystals. *J. Mater. Chem.* **20**, 9832–9847 (2010).

26. Mulder, D. J., Schenning, A. P. H. J. & Bastiaansen, C. W. M. Chiral-nematic liquid crystals as one dimensional photonic materials in optical sensors. *J. Mater. Chem. C* **2**, 6695–6705 (2014).

27. Stumpel, J. E., Broer, D. J. & Schenning, A. P. H. J. Stimuli-responsive photonic polymer coatings. *Chem. Commun.* **50**, 15839–15848 (2014).

28. Wang, D., Park, S.-Y. & Kang, I.-K. Liquid crystals: emerging materials for use in real-time detection applications. *J. Mater. Chem. C* **3**, 9038–9047 (2015).

29. Khandelwal, H., van Heeswijk, E. P. A., Schenning, A. P. H. J. & Debije, M. G. Paintable temperature-responsive cholesteric liquid crystal reflectors encapsulated on a single flexible polymer substrate. *J. Mater. Chem. C* **328**, 7395–7398 (2019).

30. Nickmans, K., van der Heijden, D. A. C. & Schenning, A. P. H. J. Photonic Shape Memory Chiral Nematic Polymer Coatings with Changing Surface Topography and Color. *Adv. Opt. Mater.* **1900592**, 1900592 (2019).

31. Van Heeswijk, E. P. A., Kragt, A. J. J., Grossiord, N. & Schenning, A. P. H. J. Environmentally responsive photonic polymers. *Chem. Commun.* **55**, 2880–2891 (2019).

32. Belmonte, A. *et al.* Dual Light and Temperature Responsive Micrometer-Sized Structural Color Actuators. *Small* **16**, (2020).

33. Belmonte, A., Pilz da Cunha, M., Nickmans, K. & Schenning, A. P. H. J. Brush-Paintable, Temperature and Light Responsive Triple Shape-Memory Photonic Coatings Based on Micrometer-Sized Cholesteric Liquid Crystal Polymer Particles. *Adv. Opt. Mater.* (2020). doi:10.1002/adom.202000054

34. Leo, S. Y. *et al.* Programmable Macroporous Photonic Crystals Enabled by Swelling-Induced All-Room-Temperature Shape Memory Effects. *Adv. Funct. Mater.* **27**, 1–11

PRIME has received Funding from the European Union's Horizon 2020 research and innovation programme under Grant Agreement No. 829010

(2017).

35. Moirangthem, M., Engels, T. A. P., Murphy, J., Bastiaansen, C. W. M. & Schenning, A. P. H. J. Photonic Shape Memory Polymer with Stable Multiple Colors. *ACS Appl. Mater. Interfaces* **9**, 32161–32167 (2017).

36. Yang, Z. *et al.* Thermal and UV shape shifting of surface topography. *J. Am. Chem. Soc.* **128**, 1074–1075 (2006).

37. Foelen, Y. *et al.* An Optical Steam Sterilization Sensor Based On a Dual-Responsive Supramolecular Cross-Linked Photonic Polymer. (2020). doi:10.1021/acsami.0c00711

38. Abramoff, M., Magalhães, P., & Ram, S. J. (2003). Image Processing with ImageJ. Biophotonics International, 11, 36-42.

PRIME has received Funding from the European Union's Horizon 2020 research and innovation programme under Grant Agreement No. 829010